

Communication

# Synthesis and X-ray Structures of Potential Light-Harvesting Ruthenium(II) Complexes

Kadarkaraisamy Mariappan <sup>\*</sup>, Anwar Hussain , Nathaniel Nisly, Tanner J. Henning, Kathryn A. Goerl, Madhubabu Alaparathi and Andrew G. Sykes

Department of Chemistry, University of South Dakota, Vermillion, SD 57069, USA

<sup>\*</sup> Correspondence: kadarkaraisamy.mariappan@usd.edu

**Abstract:** We synthesized the luminescent ruthenium(II) polypyridyl complexes of type  $[\text{Ru}(\text{bpy})_2(\text{L}1)] [\text{ClO}_4]_2$  (**1**) (where L1 = 4,4-dicarboxy-2,2-bipyridine);  $[\text{Ru}(\text{bpy})_2(\text{L}2)] [\text{ClO}_4]_2$  (**2**); and  $[\text{Ru}(\text{L}2)_3] [\text{ClO}_4]_2$  (**3**) (where L2 = 4,4-dimethanol-2,2-bipyridine). Photo-physical and electrochemical properties of the Ru(II) complexes were investigated along with the emission vs. pH. This reveals that the carboxylic acids in the 2,2-bipyridine ligand had a more important influence on the photophysical and electrochemical properties of the Ru(II) complexes than alcohol. The crystal structure of the Ru(II) complexes **1–3** is also discussed in this paper. The cyclic voltammetry of **1–3** yields a reversible Ru(III)/II wave that shifts 1.4–1.2 V. UV/Visible absorbance spectroscopy reveals that Metal-to-Ligand Charge Transfer (MLCT) transitions shift to lower energy upon deprotonation of the complex.

**Keywords:** structure determination; crystallography; X-ray diffraction; organic compound; NMR; heteroatom; organometallic; Ru(II) photosensitizers; emission; cyclic voltammetry



**Citation:** Mariappan, K.; Hussain, A.; Nisly, N.; Henning, T.J.; Goerl, K.A.; Alaparathi, M.; Sykes, A.G. Synthesis and X-ray Structures of Potential Light-Harvesting Ruthenium(II) Complexes. *Molbank* **2023**, *2023*, M1635. <https://doi.org/10.3390/M1635>

Academic Editor: R. Alan Aitken

Received: 7 March 2023

Revised: 13 April 2023

Accepted: 20 April 2023

Published: 27 April 2023



**Copyright:** © 2023 by the authors. Licensee MDPI, Basel, Switzerland. This article is an open access article distributed under the terms and conditions of the Creative Commons Attribution (CC BY) license (<https://creativecommons.org/licenses/by/4.0/>).

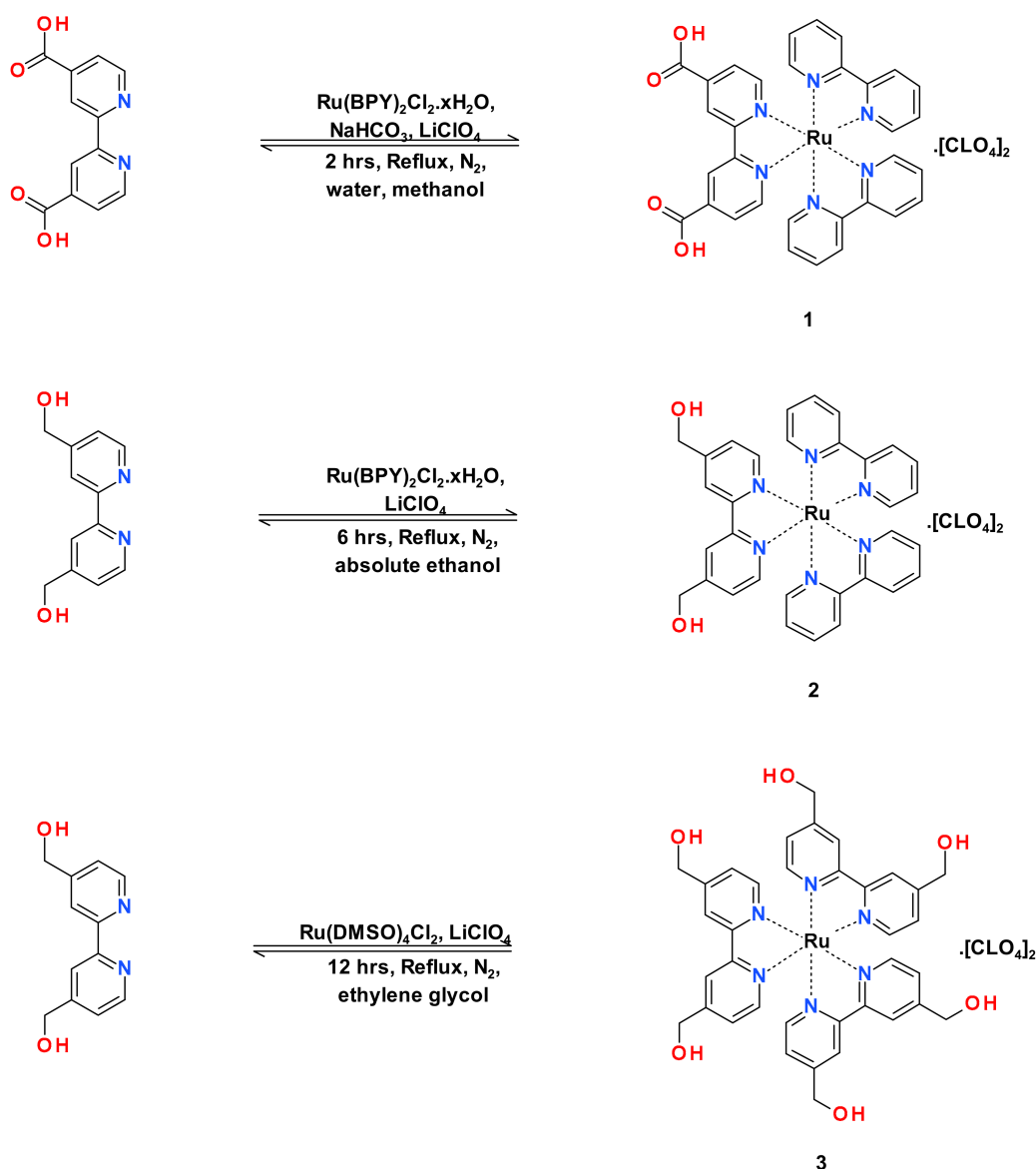
## 1. Introduction

Energy is a basic need and is essential for the earth's life [1]. The increasing consumption of non-renewable energies such as fossil fuels has caused an adverse effect on ecosystems, causing pollution and global warming, leading to a focus on sustainable and renewable energy sources [2]. Two crucial renewable energy sources have been a significant focus in the 21st century for a clean and sustainable environment: solar and hydrogen fuel cells. Solar cells use the light energy from the sun, whereas hydrogen fuel cells combine hydrogen and oxygen to produce electricity. However, the cost and non-eco-friendly waste to construct the solar cells and generate hydrogen has limited the scope of these renewable sources of energy.

Ruthenium complexes are well-known as the photosensitizer for Dyes-Sensitized Solar Cells (DSSCs) and water splitting due to their high-oxidized state stability and photo-electrochemical properties, making their practical application feasible [3]. At present, several ruthenium(II)-polypyridyl complexes have been employed as active materials for DSSCs with overall power conversation efficiencies of over 11% under standard illumination, which is attributed to a wide-absorption range (visible to near-infrared) of material [4]. The absorption range of ruthenium(II)-polypyridyl complexes can be tuned carefully to improve the optical properties by considering the HOMO and LUMO energy levels for their potential application in DSSCs.

In this regard, we have synthesized a couple of ruthenium(II)-polypyridyl complexes (*cis*- $[\text{Ru}(\text{bpy})_2(\text{bpy}-\text{X})]$ ) with different substituent groups (X = 4,4-dicarboxy-2,2-bipyridine; 4,4-methanol-2,2-bipyridine) on the 2,2-bipyridine ligand, as shown in Scheme 1, to study the effect of the substituent in photoelectric conversion. The spectroscopy and photochemistry of complexes  $[\text{Ru}(\text{bpy})_2\text{L}]_2$  have been of particular interest (for example, L = dicarboxy-4,4-bipyridine) because of their longer emission lifetimes and higher emission quantum yields. In such mixed-ligand complexes, the electron is largely localized

on that ligand, which is more easily reduced. So, bis-(2,2-bipyridine)(4,4-dicarboxy-2,2-bipyridine)ruthenium(II) perchlorate (1), bis-(2,2-bipyridine)(4,4-methanol-2,2-bipyridine)ruthenium(II) perchlorate (2) as well as tris-(4,4-methanol-2,2-bipyridine)ruthenium(II) perchlorate (3) were synthesized. Detailed studies on the properties of all the complexes are reported in this paper. In addition, the photophysical and redox properties of such transition metal complexes can provide important information regarding the nature of the ground and excited states. These experiments aimed to investigate the photophysical and electrochemical properties of these complexes.



**Scheme 1.** Reaction scheme for the synthesis of ruthenium(II) complexes (1–3).

## 2. Results and Discussion

### 2.1. NMR Spectroscopy

The  $^1\text{H}$  and  $^{13}\text{C}$  NMR spectra for compounds 1–3 were recorded in  $\text{CD}_3\text{CN}$ . Compounds 1–3 showed appropriate numbers of multiplets in the aromatic region, and the  $-\text{COOH}$  proton did not show in the  $^1\text{H}$  NMR spectrum of compound 1. Functionalized BPY's aromatic protons are de-shielded. Compounds 2 and 3 exhibited peaks at 4.74 ppm and 5.73 ppm due to the  $-\text{CH}_2\text{OH}$  group. Further, as expected, all resonances were sharp and had well-defined splitting patterns. The aromatic and aliphatic proton ratios matched well

with the proposed structure. Compounds 1–3 produced the expected number of signals in the  $^{13}\text{C}$  NMR. The NMR spectra of compounds 1–3 are shown in Figures S1–S6.

## 2.2. Crystallization and Structure Determination

The structures of  $[\text{Ru}(\text{bpy})_2\{\text{bpy}(\text{COOH})_2\}]^{2+}$  (1),  $[\text{Ru}(\text{bpy})_2\{\text{bpy}(\text{CH}_2\text{OH})_2\}]^{2+}$  (2) and  $[\text{Ru}\{\text{bpy}(\text{CH}_2\text{OH})_2\}_3]^{2+}$  (3) were studied by X-ray diffraction, as shown in Figure 1. The crystallographic data are given in Table 1, and selected bond distances and angles are listed in Table 2.

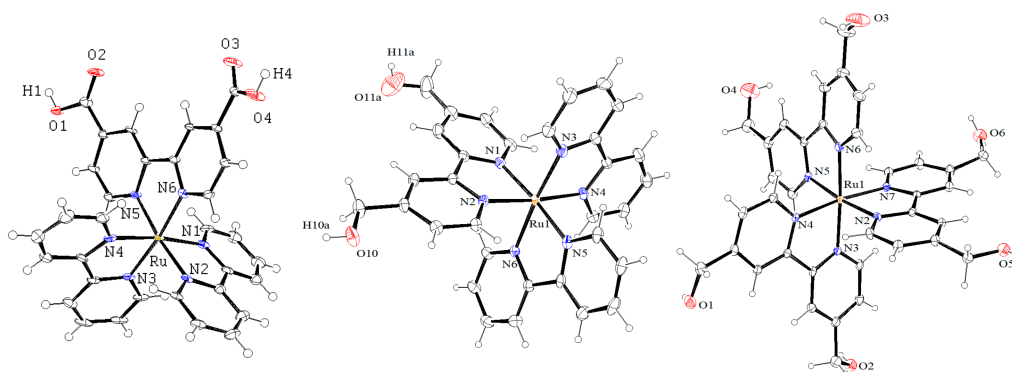


**Figure 1.** ORTEP (50% ellipsoid) of compounds 1–3. Selected atoms are labeled. Anions and solvents are not shown here for clarity.

**Table 1.** Crystallographic data for compounds 1–3.

Compounds	1	2	3
Empirical formula	$\text{C}_{38}\text{H}_{33}\text{Cl}_2\text{N}_9\text{O}_{12}\text{Ru}$	$\text{C}_{32}\text{H}_{28}\text{Cl}_2\text{N}_6\text{O}_{10}\text{Ru}$	$\text{C}_{76}\text{H}_{78}\text{N}_{14}\text{O}_{31}\text{Ru}_2\text{Cl}_4$
Formula weight	979.70	828.29	2027.46
Wavelength	MoK $\alpha$ 0.71073	MoK $\alpha$ 0.71073	MoK $\alpha$ 0.71073
System	SMART APEXII	SMART APEXII	SMART APEXII
Temperature, K	100(2)	100(2)	100(2)
Crystal system	triclinic	monoclinic	Triclinic
Space group	P-1	P 1 21 / c 1	P-1
<i>a</i> , Å	8.993(3)	8.8451(6)	10.7926(4)
<i>b</i> , Å	14.987(5)	30.857(2)	11.1969(4)
<i>c</i> , Å	15.291(5)	14.0432(9)	19.3405(8)
$\alpha$ , °	93.301(4)	90	84.03
$\beta$ , °	93.474(4)	99.2170(10)	80.87
$\gamma$ , °	97.352(4)	90	62.94
Volume, Å <sup>3</sup>	2035.8(12)	3783.4(4)	2053.54(14)
Z	2	8	1
Density (calc) g·cm <sup>-3</sup>	1.598	1.441	1.639
Absorb. Coef. Mm <sup>-1</sup>	0.591	0.615	1036
<i>F</i> (000)	996	1663	1036
$\theta$ range	2.51–24.08	2.42–24.86	2.26–27.27
Index ranges	$\pm 10, \pm 17, \pm 17$	$\pm 10, \pm 37, \pm 16$	$\pm 13, \pm 14, \pm 24$
Reflections collected	18331	38991	24520
Independent reflections	6538	6986	9261
Observed reflections	5311	5610	7809
Max/Min trans.	0.737–0.943		0.866–0.943
Data/restr./param.	6538/0/562	6986/2/462	9261/0/582
Goodness-of-fit	1.067	1.107	1.071
Final R indices [ <i>I</i> > 2 $\sigma$ ( <i>I</i> )]	0.0390	0.0522	0.0623
R indices (all data)	0.0539	0.0640	0.0751
CCDC Number	1443902	1857593	1857586

**Table 2.** Important bond lengths (Å) and angles (°) of compounds 1–3.

	1	2	3
C=O (double bond)	1.198 Å; 1.199 Å	-	-
C-O (single bond)	1.311 Å; 1.346 Å	1.279 Å; 1.404 Å	1.385 Å (avg)
Ru-N (avg)	2.065 Å	2.056 Å	2.058 Å
N-Ru-N (avg) (bite angle)	78.20°	78.82°	78.60°
N-Ru-N (avg) (other angles)	92.08° & 172.81°	92.08° & 174.30°	93.07° & 174.00°

The crystal structure of **1** has previously been reported without counter-ions or heavily hydrated with different cell parameters, and ruthenium(II) has been reported to be balanced by the deprotonation of carboxylic acid [5–7]. In this case, the ruthenium(II) of complex **1** was balanced with the presence of perchlorate anions as counter-ions and solvated with acetonitrile (Figure S10). The bond length of C=O (1.199 Å), C-O (1.328 Å), average Ru-N distance (2.065 Å), average bite angle of N-Ru-N (78.70°), and other average angles of N-Ru-N (92.08° and 172.81°) are similar to the crystal structure reported previously [5].

The crystal structure of **2** has previously been reported with different cell parameters, with hexafluorophosphate as counter-ions and as solvated with water and acetone [8]. The average bond length of C-O (1.341 Å), average Ru-N distance (2.056 Å), average bite angle of N-Ru-N (78.82°), and other average angles of N-Ru-N (92.08° and 174.30°) are similar to those reported for other bipyridyl-coordinated [Ru(bpy)<sub>3</sub>]<sup>2+</sup> and [Ru(bpy)<sub>2</sub>(bpy(OH)<sub>2</sub>)]<sup>2+</sup> complexes [5,9,10]. Here, the ruthenium(II) is balanced with the two perchlorate anions.

The crystal structure of **3** is reported here for the first time. The average bond length of C-O, average Ru-N length, average bite angle, and other angles of N-Ru-N of **3** are presented in Table 1 and are found to be similar to the crystal structure of **2**. However, the three hydroxymethyl groups are disordered; ruthenium(II) is balanced with two perchlorate anions and solvated with acetonitrile and water molecules.

### 2.3. Optical Properties

#### 2.3.1. Absorbance Spectroscopy

UV/Visible absorption data were collected for **1**, **2**, and **3** using a  $5 \times 10^{-5}$  molar solution in water (Figure 2). The observed absorbance bands were like those seen for [Ru(bpy)<sub>3</sub>]<sup>2+</sup> in water. Several intense transitions in the wavelength range from 240 to 300 nm are assigned to  $\pi$ - $\pi^*$  transitions. The electronic transitions that appear at wavelengths higher than 300 nm in [Ru(bpy)<sub>3</sub>]<sup>2+</sup> result from many overlapping MLCT bands from the metal-centered d-orbitals to the ligand  $\pi^*$  orbitals and are, therefore, assigned similarly for **1**–**3**. The lowest energy MLCT transition observed for compounds **1**–**3** occurs at  $\lambda_{\max} = \sim 460$  nm, which are like the corresponding MLCT transitions in [Ru(bpy)<sub>3</sub>]<sup>2+</sup> ( $\lambda_{\max} = 451$  nm). Compound **1**'s MLCT band is slightly more red-shifted than compounds **2** and **3** due to the electron-withdrawing –COOH group.

These wavelength shifts scale with the ligands' electron-donating ability, which destabilizes the filled d-orbitals, resulting in lower transition energies. In addition, these results follow the same trend observed for the RuIII/II redox potential as a function of ligands. Upon deprotonation of **2**–**3** with aqueous *t*-butylammonium hydroxide or aqueous NaOH in an aqueous solution to make –CH<sub>2</sub>O<sup>–</sup>, the spectral region between 300 and 600 nm did not change significantly, as shown in Figures S11 and S12.

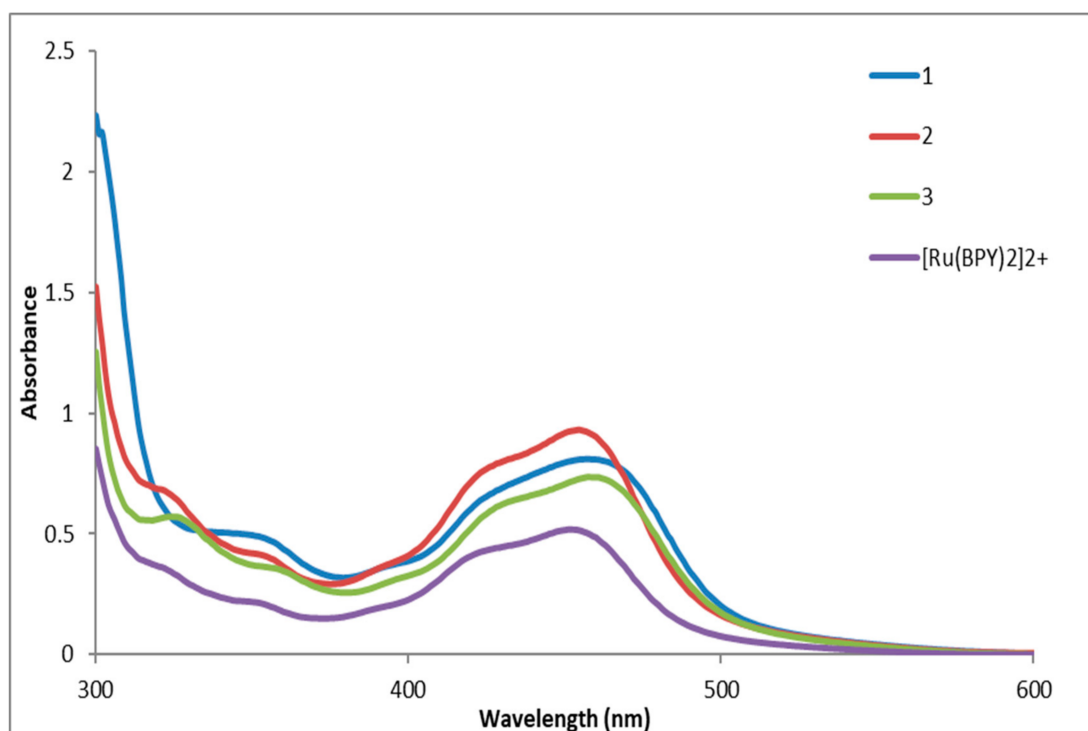


**Figure 2.** UV spectrum of compounds 1–3. A  $5 \times 10^{-5}$  molar of 1–3 in water was used for the studies.

### 2.3.2. Emission Spectroscopy

The emission spectra of 1–3 (Figure 3) in acetonitrile showed a nice Gaussian curve with an emission maximum at 660 nm, 610 nm, and 618 nm, respectively. Compound 2's emission is ~50 nm more blue-shifted than compound 1 due to the  $-\text{CH}_2\text{OH}$  group. The emission maximum of compound 3 is close to compound 1.

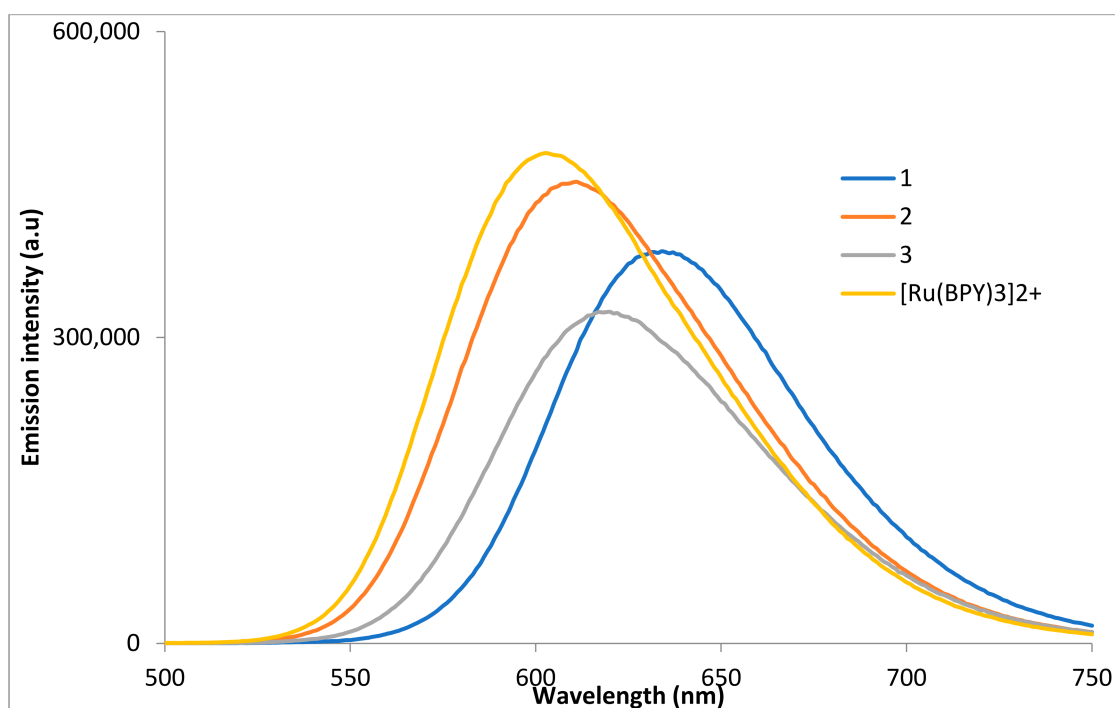


**Figure 3.** Emission spectra of compounds 1–3. A  $5 \times 10^{-5}$  molar of 1–3 in water was used for the studies, and the excitation wavelength = 450 nm.

## 2.4. Cyclic Voltammetry

It is important to know the details of the redox process of  $\text{Ru}^{3+/2+}$  to understand the redox chemistry of the ruthenium complexes 1–3, which is presented in Figures S7–S9. The redox chemistry of complexes 1–3 in  $\text{CH}_3\text{CN}$  is presented in Table 3 as compared with  $\text{Ru}(\text{bpy})_3^{2+}$ . The cyclic voltammogram of  $\text{Ru}(\text{bpy})_3^{2+}$  corresponds to the reversible one metal-based  $\text{Ru}^{3+/2+}$  oxidation process and three one-electron BPY-based reduction processes [11]. We observe similar redox chemistry for all complexes; however, in compound 3, the three one-electron reduction processes are merged together into a single broad peak at  $-1.34$  V, as shown in Figure 4, which is due to the effect of the substituent in the bipyridine unit.

**Table 3.** Electrochemical data; referenced vs. Ag/AgCl, glassy carbon, 1 mM in 0.1 M tetrabutylammonium perchlorate at room temperature.

Compound	Solvent	$E_{1/2}^A$ (V)			
		BPY <sup>0/−1</sup>	BPY reduction BPY <sup>−1/−2</sup>	BPY <sup>−2/−3</sup>	Oxidation Ru <sup>3+/2+</sup>
1	$\text{CH}_3\text{CN}$	−1.39	−1.58	−1.87	+1.38
2	$\text{CH}_3\text{CN}$	−1.31	−1.48	−1.736	+1.29
3	$\text{CH}_3\text{CN}$		−1.34		+1.19
$([\text{Ru}(\text{bpy})_3]^{2+})$ [11]	$\text{CH}_3\text{CN}$	−1.31	−1.50	−1.77	+1.27

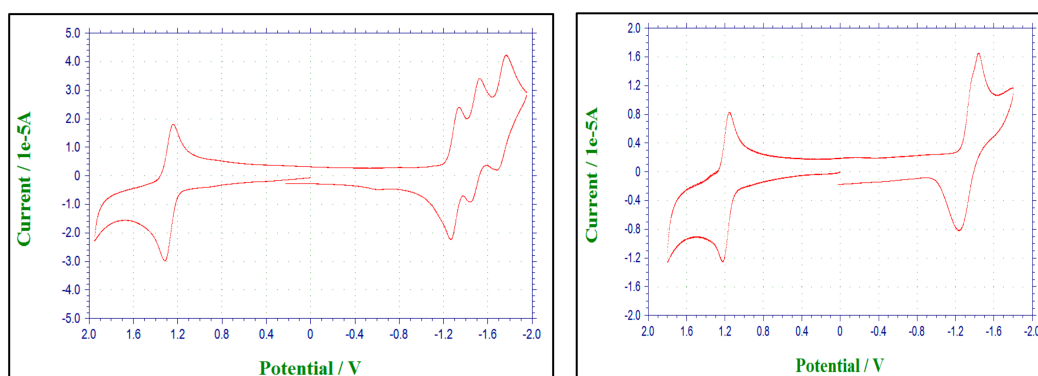


**Figure 4.** Cyclic voltammogram of compounds 2 and 3. Referenced vs. Ag/AgCl, glassy carbon, 1 mM in 0.1 M tetrabutylammonium perchlorate.

In mixed-ligand complexes such as compounds 1–2, these electron transitions upon optical absorption would occur between the metal center and the ligand, which is most easily reducible. The electron-withdrawing character of the carboxylic acid group would shift the reduction potential of the ligand positively relative to that of the unsubstituted BPY ligand, as reported earlier [12]. Furthermore, compound 1 showed a promising applicability<sup>10</sup> towards Dye-Sensitized Solar Cells. From 1 to 3, the oxidation potentials decreased with an increasing pKa. The data presented in Table 3 on the complexes with carboxylic acid groups and alcoholic functional groups exposes several interesting effects on the Ru→L luminescence.

## 3. Materials and Methods

### 3.1. Materials

4,4'-bis(hydroxymethyl)-2,2'-bipyridine, 4,4'-dicarboxy-2,2'-bipyridine,  $[\text{Ru}(\text{BPY})_2\text{Cl}_2] \cdot x\text{H}_2\text{O}$ , lithium perchlorate, tetrabutylammonium perchlorate (TBAP), tetrabutylammonium hydroxide and 70% perchloric acid were purchased from Aldrich and used without purification. The perchlorate salts used in the selectivity studies were dried at 100 °C under a vacuum over Drierite to minimize the effects of hydration.  $\text{CH}_3\text{CN}$ , THF, DMF, and  $\text{CH}_2\text{Cl}_2$  were purchased from Aldrich and purified using a PURE SOLV<sup>TM</sup> solvent

purification system. HPLC-grade anhydrous acetonitrile (Fisher/Acros) was used in all spectroscopic studies.

*Caution: Although we have experienced no difficulties with these perchlorate salts, they should be treated as potentially explosive and handled with care.*

### 3.2. Physical Measurements

The  $^1\text{H}$  and  $^{13}\text{C}$  NMR spectra were obtained using Bruker 400 MHz instruments at room temperature and using deuterated solvents. Absorbance data were collected using a Varian Cary 50 BIO UV-visible spectrophotometer. Luminescence titrations were conducted using a Fluoromax-4 spectrofluorometer. Mass spectrometry was conducted using a Varian 500-MS IT ESI mass spectrometer. The cyclic voltammograms were recorded using a CH instruments 660 electrochemical workstation. Elemental analyses were conducted using an Exeter CE-440 Elemental analyzer. Melting points were determined using open capillaries and were uncorrected.

### 3.3. Single-Crystal X-ray Structure Determination

X-ray quality crystals of compounds 1–3 was obtained by the diffusion of diethyl ether into an acetonitrile solution. Crystallographic data for 1–3 was collected at 100 K using a Bruker SMART APEX II diffractometer by  $\text{MoK}\alpha$  radiation. The data reduction and refinement were completed using the WinGX suite of crystallographic software [13,14]. Structures were solved using SIR97 [15]. All hydrogen atoms were placed in ideal positions and refined as riding atoms with relative isotropic displacement parameters. Table 1 lists additional crystallographic and refinement information.

### 3.4. Experimental Procedure

#### Synthesis of Ruthenium(II) Complexes (1–3)

##### **Synthesis of [bis(2,2'-bipyridine)(4,4'-dicarboxy-2,2'-bipyridine)ruthenium(II)] perchlorate (1):**

A slight modification was done in the available procedure<sup>9</sup> to synthesize compound 1. A total of 1-g (1.85 mmol) of  $\text{Ru}(\text{BPY})_2\text{Cl}_2 \cdot x\text{H}_2\text{O}$  was mixed with little excess (0.6 g, 2.55 mmol) of 4,4'-dicarboxyl-2,2'-bipyridine along with 0.6 g (7.14 mmol) of sodium bicarbonate in a round bottom flask. The solution was refluxed in 30 mL of water and 20 mL of methanol for 2–3 h under an inert atmosphere. It cooled down on its own after the heating period. A saturated aqueous lithium perchlorate was added to the reaction mixture, and the solution was brought to acidic levels (pH = 5–6) using 70% perchloric acid. Red powder with very high purity obtained over time was filtered and dried under a vacuum. The yield is 70%, and the melting point is over 300 °C. A small portion of the red powder was dissolved in acetonitrile, and diethyl ether was diffused into the solution. Dark red crystals of complex 1 were obtained over time. The elemental analyses calculated for  $\text{C}_{32}\text{H}_{24}\text{N}_6\text{O}_{12}\text{RuCl}_2 \cdot 3\text{CH}_3\text{CN}$  included: C, 46.59; H, 3.37; and N, 12.86 %. The following further values were found: C, 46.17; H, 3.21; and N, 12.47 %. The following were found for  $^1\text{H}$  NMR ( $\text{CD}_3\text{CN}$  at 25 °C): 7.39–7.45 (m, 4H, Ar-H); 7.61–7.72 (m, 4H, Ar-H); 7.81–7.83 (m, 2H, Ar-H); 7.93–7.95 (m, 2H, Ar-H); 8.05–8.11 (m, 4H, Ar-H); 8.51–8.53 (m, 4H, Ar-H); and 9.03 (s, 2H, Ar-H). The following were found for  $^{13}\text{C}$  NMR ( $\text{CD}_3\text{CN}$  at 25 °C): 124.9, 125.4, 127.8, 128.7, 128.8, 139.3, 139.8, 152.6, 152.8, 153.8, 157.6, 157.8, 158.7, and 165.1.

##### **Synthesis of [bis(2,2'-bipyridine)(4,4'-bis(hydroxymethyl)-2,2'-bipyridine)ruthenium(II)] perchlorate (2):**

$\text{Ru}(\text{BPY})_2\text{Cl}_2 \cdot x\text{H}_2\text{O}$  (0.5 g, 0.93 mmol) was mixed with 0.22 g (1.01 mmol) of 4,4'-bis(hydroxymethyl)-2,2'-bipyridine in a round bottom flask that contained 50 mL of absolute ethanol. The solution was refluxed for 6 h under an inert atmosphere and cooled down to room temperature. A saturated aqueous lithium perchlorate was added to the reaction mixture, and the solution was kept in the refrigerator. Red powder was obtained over time, filtered, and dried under a vacuum. The yield was 65%, and the melting point was over 250 °C. The red powder was dissolved in a minimum amount of acetonitrile, and diethyl

ether was diffused into the solution. Orange-red crystals of complex **2** were obtained over time. The elemental analyses were calculated for  $C_{32}H_{28}N_6O_{10}RuCl_2 \cdot CH_3CH_2OCH_2CH_3$  included: C, 46.39; H, 3.38; and N, 10.14 %. The following further values were found: C, 46.26; H, 3.30; and N, 9.98 %. The following were found for  $^1H$  NMR ( $CD_3CN$  at 25 °C): 4.73–4.75 (*d*, 2H,  $CH_2-O$ ); 5.72–5.74 (*t*, 2H, OH); 7.45–7.54 (*m*, 6H, Ar-H); 7.64–7.66 (*m*, 2H, Ar-H); 7.73–7.76 (*m*, 4H, Ar-H); 8.14–8.18 (*m*, 4H, Ar-H); 8.69 (*s*, 2H, Ar-H); and 8.82–8.84 (*m*, 4H, Ar-H). The following were found for  $^{13}C$  NMR ( $CD_3CN$  at 25 °C): 61.2; 121.3; 124.4; 124.9; 137.8; 150.7; 151.1; 151.2; 154.3; 156.0; and 156.6.

#### Synthesis of [(4,4'-bis(hydroxymethyl)-2,2'-bipyridine)ruthenium(II)] perchlorate (**3**):

$Ru(DMSO)_4Cl_2$  (0.3 g, 0.62 mmol) was mixed with a 3.3 equivalent of 4,4'-bis(hydroxymethyl)-2,2'-bipyridine (0.42 g) in a round bottom flask that contained 30 mL of ethylene glycol. The solution was refluxed overnight under an inert atmosphere and cooled down to room temperature. A saturated aqueous lithium perchlorate was added to the reaction mixture, and the solution was kept in the refrigerator. Red powder was obtained over time, filtered, and dried under a vacuum. The yield was 50%, and the melting point was over 250 °C. The red powder was dissolved in a minimum amount of acetonitrile, and diethyl ether was diffused into the solution. Red crystals of complex **3** were obtained over time. The elemental analyses were calculated for  $C_{36}H_{42}N_6O_{14}RuCl_2$  included: C, 45.30; H, 4.40; and N, 8.80 %. The following further values were found: C, 45.17; H, 4.31; and N, 8.65 %. The following were found for  $^1H$  NMR ( $CD_3CN$  at 25 °C): 3.96–3.99 (*t*, 2H, OH); 4.77–4.79 (*d*, 2H,  $CH_2-O$ ); 7.45–7.54 (*d*, 6H, Ar-H); 7.33–7.35 (*d*, 6H, Ar-H); and 8.47 (*s*, 6H, Ar-H). The following were found for  $^{13}C$  NMR ( $CD_3CN$  at 25 °C): 62.6; 122.2; 125.6; 152.1; 154.8; and 157.8.

## 4. Conclusions

The ruthenium(II) polypyridyl complexes were synthesized and characterized using spectroscopic and electrochemical techniques. The photo-physical and electrochemical properties of the Ru(II) complexes reveal the influence of substituents on 2,2'-bipyridine. The DSSC property of compound **1** was tested and reported, and we are currently exploring the application of compounds **2** and **3** as well. The cyclic voltammetry of complexes **1–3** reveals the  $Ru^{3+/2+}$  oxidation wave that shifts 1.4–1.2 V to lower energy levels, whereas the Metal-to-Ligand Charge Transfer (MLCT) transitions shift to lower energy levels upon deprotonation of the complex. This observation contrasts with mixed-ligand systems containing deprotonate groups, such as  $-CH_2OH$ , that demonstrate different types of electronic transitions assigned as mixed Metal-Ligand-to-Ligand Charge Transfer (MLCT).

**Supplementary Materials:** The following supporting information can be downloaded online. Figure S1.  $^1H$  NMR of compound **1**. Figure S2.  $^1H$  NMR of compound **2**. Figure S3.  $^1H$  NMR of compound **3**. Figure S4.  $^{13}C$  NMR of compound **1**. Figure S5.  $^{13}C$  NMR of compound **2**. Figure S6.  $^{13}C$  NMR of compound **3**. Figure S7. CV of compound **1**. Referenced vs. Ag/AgCl, glassy carbon, 1 mM in 0.1 M tetrabutylammonium perchlorate. Figure S8. CV of compound **2**. Referenced vs. Ag/AgCl, glassy carbon, 1 mM in 0.1 M tetrabutylammonium perchlorate. Figure S9. CV of compound **3**. Referenced vs. Ag/AgCl, glassy carbon, 1 mM in 0.1 M tetrabutylammonium perchlorate. Figure S10. ORTEP of compound **1**, along with solvents and anions. Figure S11. UV and emission spectra of **1–3** ( $5 \times 10^{-5}$  M) in water with an excess of tetrabutylammonium hydroxide and the excitation wavelength = 450 nm. Figure S12. UV and emission spectra of **1–3** ( $5 \times 10^{-5}$  M) in water with an excess of sodium hydroxide, and the excitation wavelength = 450 nm.

**Author Contributions:** Conceptualization, K.M. and A.G.S.; methodology, K.M.; software, A.H. and M.A.; validation, K.M., A.H. and M.A.; formal analysis, N.N., T.J.H. and K.A.G.; investigation, N.N., T.J.H. and K.A.G.; resources, K.M.; data curation, N.N., T.J.H. and K.A.G.; writing—original draft preparation, K.M.; writing—review and editing, A.H.; visualization, K.M.; supervision, K.M.; project administration, K.M.; funding acquisition, A.G.S. All authors have read and agreed to the published version of the manuscript.

**Funding:** N.N., T.J.H. and K.A.G. gratefully acknowledge support for summer REU (NSF CHE 1460872) research at USD. NSF-EPSCoR (EPS-0554609) and the South Dakota Governor's 2010 Initiative are also appreciated for the purchase of a Bruker SMART APEX II CCD diffractometer. NSF-URC (CHE-0532242) also provided funding for the purchase of the elemental analyzer. The 400 MHz Bruker NMR was also provided by funding from NSF-MRI-CHE-1229035. The authors would like to thank the Center for Fluorinated Functional Materials (CFFM) for financial support and NSF-MRI-CHE-1919637 for the purchase of a Bruker Dual-Source Single-Crystal X-ray Diffractometer.

**Institutional Review Board Statement:** Not applicable.

**Informed Consent Statement:** Not applicable.

**Data Availability Statement:** The crystallographic data (CCDC entry: 1443902, 1857593, 1857586) can be obtained free of charge via [www.ccdc.cam.ac.uk/conts/retrieving.html](http://www.ccdc.cam.ac.uk/conts/retrieving.html) and can be accessed on or after 1 August 2023 (or from the Cambridge Crystallographic Data Centre, 12, Union Road, Cambridge CB21EZ, UK; fax: +44-1223-336-033; or [deposit@ccdc.cam.ac.uk](mailto:deposit@ccdc.cam.ac.uk)). Supplementary information is available on the journal website as a softcopy.

**Conflicts of Interest:** The authors declare no conflict of interest.

## References

1. Lior, N. Energy resources and use: The present situation and possible paths to the future. *Energy* **2008**, *33*, 842–857. [[CrossRef](#)]
2. Qin, Y.; Peng, Q. Ruthenium sensitizers and their applications in dye-sensitized solar cells. *Int. J. Photoenergy* **2012**, *2012*, 842–857. [[CrossRef](#)]
3. Kohle, O.; Grätzel, M.; Meyer, A.F.; Meyer, T.B. The photovoltaic stability of, bis (isothiocyanato) ruthenium (II)-bis-2, 2'-bipyridine-4, 4'-dicarboxylic acid and related sensitizers. *Adv. Mater.* **1997**, *9*, 904–906. [[CrossRef](#)]
4. Nazeeruddin, M.K.; Pechy, P.; Renouard, T.; Zakeeruddin, S.M.; Humphry-Baker, R.; Comte, P.; Liska, P.; Cevey, L.; Costa, E.; Shklover, V. Engineering of efficient panchromatic sensitizers for nanocrystalline TiO<sub>2</sub>-based solar cells. *J. Am. Chem. Soc.* **2001**, *123*, 1613–1624. [[CrossRef](#)] [[PubMed](#)]
5. Beauvilliers, E.E.; Meyer, G.J. Evidence for Cation-Controlled Excited-State Localization in a Ruthenium Polypyridyl Compound. *Inorg. Chem.* **2016**, *55*, 7517–7526. [[CrossRef](#)] [[PubMed](#)]
6. Caspar, R.; Amouri, H.; Gruselle, M.; Cordier, C.; Malézieux, B.; Duval, R.; Leveque, H. Efficient asymmetric synthesis of  $\Delta$ - and  $\Lambda$ -enantiomers of (bipyridyl) ruthenium complexes and crystallographic analysis of  $\Delta$ -bis (2, 2'-bipyridine)(2, 2'-bipyridine-4, 4'-dicarboxylato) ruthenium: Diastereoselective homo- and heterochiral ion pairing revisited. *Eur. J. Inorg. Chem.* **2003**, *2003*, 499–505.
7. Pang, J.; Di, Z.; Qin, J.-S.; Yuan, S.; Lollar, C.T.; Li, J.; Zhang, P.; Wu, M.; Yuan, D.; Hong, M. Precisely embedding active sites into a mesoporous Zr-framework through linker installation for high-efficiency photocatalysis. *J. Am. Chem. Soc.* **2020**, *142*, 15020–15026. [[CrossRef](#)] [[PubMed](#)]
8. Guillo, P.; Hamelin, O.; Pécaut, J.; Ménage, S. Complexation to [Ru (bpy)<sub>2</sub>]<sup>2+</sup>: The trick to functionalize 3, 3'-disubstituted-2, 2'-bipyridine. *Tetrahedron Lett.* **2013**, *54*, 840–842. [[CrossRef](#)]
9. Rillema, D.P.; Jones, D.S. Structure of tris (2, 2'-bipyridyl) ruthenium (II) hexafluorophosphate, [Ru(bipy)<sub>3</sub>][PF<sub>6</sub>]<sub>2</sub>; X-ray crystallographic determination. *J. Chem. Soc. Chem. Commun.* **1979**, *19*, 849–851. [[CrossRef](#)]
10. Hansen, L.E.; Glowacki, E.R.; Arnold, D.L.; Bernt, G.J.; Chi, B.; Fites, R.J.; Freeburg, R.A.; Rothschild, R.F.; Krieg, M.C.; Howard, W.A. Syntheses and characterization of some chloro, methoxy, and mercapto derivatives of [Ru ( $\eta^2$ -2, 2'-bipyridine)<sub>3</sub>]<sup>2+</sup> 2PF<sub>6</sub><sup>-</sup>: Crystal and molecular structures of [Ru ( $\eta^2$ -2, 2'-bipyridine) 2 ( $\eta^2$ -4, 4'-(X) 2-2, 2'-bipyridine)]<sup>2+</sup> 2PF<sub>6</sub><sup>-</sup> (X = Cl, OCH<sub>3</sub>). *Inorg. Chim. Acta* **2003**, *348*, 91–96. [[CrossRef](#)]
11. Rillema, D.P.; Allen, G.; Meyer, T.; Conrad, D. Redox properties of ruthenium (II) tris chelate complexes containing the ligands 2, 2'-bipyridine, 2, 2'-bipyridine, and 2, 2'-bipyrimidine. *Inorg. Chem.* **1983**, *22*, 1617–1622. [[CrossRef](#)]
12. Fuentes, M.J.; Bognanno, R.J.; Dougherty, W.G.; Boyko, W.J.; Kassel, W.S.; Dudley, T.J.; Paul, J.J. Structural, electronic and acid/base properties of [Ru (bpy (OH)<sub>2</sub>)<sub>3</sub>]<sup>2+</sup> (bpy(OH)<sub>2</sub> = 4, 4'-dihydroxy-2, 2'-bipyridine). *Dalton Trans.* **2012**, *41*, 12514–12523. [[CrossRef](#)] [[PubMed](#)]
13. Farrugia, L.J. WinGX suite for small-molecule single-crystal crystallography. *J. Appl. Crystallogr.* **1999**, *32*, 837–838. [[CrossRef](#)]
14. Sheldrick, G.M. *SHELXL-97. Program for Crystal Structure Refinement*; ScienceOpen, Inc.: Burlington, MA, USA, 1997.
15. Altomare, A.; Burla, M.C.; Camalli, M.; Cascarano, G.L.; Giacovazzo, C.; Guagliardi, A.; Moliterni, A.G.; Polidori, G.; Spagna, R. SIR97: A new tool for crystal structure determination and refinement. *J. Appl. Crystallogr.* **1999**, *32*, 115–119. [[CrossRef](#)]

**Disclaimer/Publisher's Note:** The statements, opinions and data contained in all publications are solely those of the individual author(s) and contributor(s) and not of MDPI and/or the editor(s). MDPI and/or the editor(s) disclaim responsibility for any injury to people or property resulting from any ideas, methods, instructions or products referred to in the content.